中国激光

抗血栓药物拜瑞妥的远红外光谱研究

魏小柯，吴旭*，陆小森，王俊杰，李婧楠，杨颜锶，褚欣博，王奇亮，金钻明，彭滟
上海理工大学光电信息与计算机工程学院，上海 200093

摘要 以治疗血栓的新型药物拜瑞妥为例，利用远红外光谱，实现了药物快速准确的定量分析。首先，基于密度泛函理论进行理论仿真，分析了拜瑞妥基团结构的振动模式，预测其在0～100 cm^{-1}波数范围内存在多种共振吸收。接着，利用远红外光谱仪对拜瑞妥进行检测，获得了与理论仿真结果高度一致的实验谱图，明确了拜瑞妥在远红外频段的特征吸收峰。最后，对不同质量拜瑞妥样品进行了测试，研究了拜瑞妥的特征吸收峰强度与其质量之间的线性关系，以多个特征峰为指标进行联合分析，实现了拜瑞妥药物含量的快速定量分析。研究结果有助于推动相关抗血栓药物的快速检测手段的发展。

关键词 医用光学；远红外光谱；拜瑞妥；定量检测；密度泛函理论
中图分类号 O436 **文献标志码** A **DOI**：10.3788/CJL230523

1 引 言

深静脉血栓形成（DVT）是一种发病率高达66%～84%[1]的骨科术后并发症。形成的血栓一旦脱落，会随血液循环，堵塞血管，严重时可发展为肺栓塞，导致病人残疾甚至死亡[2-4]。因此，预防血栓形成是骨科术后治疗的重要关卡，对病人术后康复至关重要。目前，治疗血栓的首选方案是口服抗凝血药物[5]。拜瑞妥（Xarelto）是临床上最常使用的新型口服抗凝药物[6-7]，通过抑制呈游离状态和呈结合状态的Xa因子（一种丝氨酸蛋白酶）实现抗凝。根据文献[6-9]可知，拜瑞妥能够有效减少骨科患者术后静脉血栓的形成，使血栓风险降低至30%。但由于病人的生理条件不同，在临床治疗中需要针对个体用药进行定量检测，以达到更好的治疗效果[10]。

目前，拜瑞妥的定量检测方法主要有两类：1）直接检测法，以高效液相色谱串联质谱法（LC-MS/MS）为代表。LC-MS/MS[11]采用液相色谱分流样本，通过一级质谱仪和二级质谱仪进行定性分析，筛选目标离子，实现定量检测。但其预处理的步骤繁琐，耗时较长，仪器和试剂成本高，不适合临床大范围使用。2）间接检测法，主要包括抗Xa因子活性检测法和凝血酶原时间检测法。其中，抗Xa因子活性检测法[12]利用紫外可见光光谱检测Xa因子，间接反映抗凝血药物的含量，但由于该方法中标准化校准的试剂较特殊、符合相关标准的实验室数量较少，目前临床上对其检测准确性仍存在争议。传统凝血酶原时间检测法[13]通过在无血小板的血浆中加入组织凝血酶原和钙离子，测量血浆凝固时间，间接反映待测物含量。但该方法受病人的生理特征、仪器和试剂的影响，难以规定统一的参考值。因此，研究者仍在寻找新型检测方式以实现拜瑞妥药物含量的快速定量研究。

远红外辐射（FIR）是波长为25～1000 μm的电磁辐射，介于中红外光与微波之间，对分子的构型变化、晶体变化、分子间作用力变化等相关低频振动或转动信息具有高灵敏性[14-15]。并且，远红外光谱检测具有光子能量低、分辨率高、谱带宽的特点，因此在分子定性鉴别和定量分析领域中得到广泛应用[16-18]。目前，远红外光谱技术已被用于多种药物的检测分析，如惊厥药物卡马西平[19]、多晶药物和非晶药物形态的检测和定量分析等[20-21]，但目前拜瑞妥的远红外光谱特性及其定量分析研究较少。

本文通过理论仿真法和实验测试法研究了拜瑞妥药物的远红外光谱特性，并基于其特性进行了定量分析。具体来说，基于密度泛函理论（DFT），分析了拜瑞妥在0～100 cm^{-1}波数范围内的吸收频率以及相关分子运动模式，预测了拜瑞妥的远红外吸收特性。利用傅里叶远红外光谱仪采集了拜瑞妥的实验吸收谱，通过对比理论分析结果，明确了拜瑞妥在远红外波段的特征峰。基于多个特征峰，研究了不同质量拜瑞妥样本在远红外波段的吸收谱的变化规律，分析了拜瑞妥质量与峰强之间的相关性，从而实现了对拜瑞妥的定量检测。

收稿日期：2023-02-14；**修回日期**：2023-03-12；**录用日期**：2023-04-03；**网络首发日期**：2023-04-13
基金项目：国家自然科学基金（61805140，61922059，81961138014）、上海市国内科技合作重点项目（21015800200）
通信作者：*wuxu@usst.edu.cn

2 材料与方法

2.1 材料

本文所采用的材料为纯度(质量分数)大于99%的拜瑞妥、粒径为40~48 μm的高密度聚乙烯(PE)、无水且纯度(质量分数)≥99.9%的二甲基亚砜。上述材料在使用前未作进一步提纯处理。

拜瑞妥定性实验样本制备:将300 mg PE分别与25 mg和60 mg药物粉末混合研磨,在3 MPa压力下制成直径为13 mm的光滑薄片。

拜瑞妥定量实验样本制备:制备步骤同上,将300 mg的PE分别与2.5、5.0、7.5、10.0、12.5、25.0 mg药物粉末混合研磨,制成直径为13 mm的光滑薄片。

压片制备过程中质量损失控制在1%以下。制备好后样本保存在一个密封干燥箱内(湿度小于3%),避免吸收空气中的水汽。

2.2 方法

2.2.1 理论仿真法

本文以PubChem Structure数据库中拜瑞妥的模型为基础,构造分子仿真模型。计算使用量子化学软件Gaussian 09。该计算软件是目前计算化学领域内最流行、应用范围最广的综合性量子化学计算程序包,可用于分子能量和结构、分子轨道、振动频率等的理论计算[22-23]。该软件的计算结果已得到大量实验的检验和认证,结果较为可靠。计算采用密度泛函理论方法,其基本原理是将一个分子看作是一个由诸多相互作用粒子组成的系统,将系统的波函数替换为粒子密度函数,利用基态密度的泛函或者电子密度分布近似解进行性质解析。该方法已被广泛用于多种分子光谱特性的预测及分子振动模式的分析,如多糖大分子阿拉伯半乳聚糖(AG)、硫酸盐阿拉伯半乳聚糖(硫酸盐)[24]、非刚性分子噻虫胺($C_6H_8ClN_5O_2S$)、呋喃二胺($C_7H_{14}N_4O_3$)[25]等,计算效率高,大多数情况下与实验数据相比误差较小[20]。因此,本文采用密度泛函理论方法对拜瑞妥远红外光谱特性进行理论仿真。具体选用DFT/B3LYP/3-21G基组,对拜瑞妥分子模型进行结构优化和频率计算,预测拜瑞妥在0~100 cm^{-1}波数范围内的分子运动模式,并对其进行高斯展宽(半峰全宽为4 cm^{-1})以得到拜瑞妥的理论光谱图。

2.2.2 实验测试法

远红外光谱均通过傅里叶变换远红外光谱仪(FTIR)采集。该设备信噪比为55000:1。检测时,样本仓为真空环境,减少了水汽对实验结果的影响,单次光谱扫描平均次数为64,光谱分辨率设为2 cm^{-1}。

本文采用纯PE及25 mg和60 mg拜瑞妥样品压片进行拜瑞妥的定性实验测试。用2.5~25.0 mg拜瑞妥与300 mg PE混合压片进行定量实验。对所有样品进行检测,采集远红外吸收图谱。

3 分析与讨论

3.1 拜瑞妥的理论仿真分析

拜瑞妥的分子结构式如图1(a)所示,分子式为$C_{19}H_{18}ClN_3O_5S$,相对分子质量为435.88。分子包含两个六元环、两个五元环以及三个醛基。两个六元环分别是苯环及N和O原子掺杂的六元环,两个五元环分别是N和O原子掺杂的五元环及S原子掺杂的五元环。通过DFT/B3LYP/3-21G基组理论计算,得到拜瑞妥在0~100 cm^{-1}波数范围内的振动模式和理论光谱。从图1(b)可明显看到拜瑞妥在该频段内有5个明显的吸收峰,分别位于24.00、40.22、72.63、81.38、100.60 cm^{-1}处。

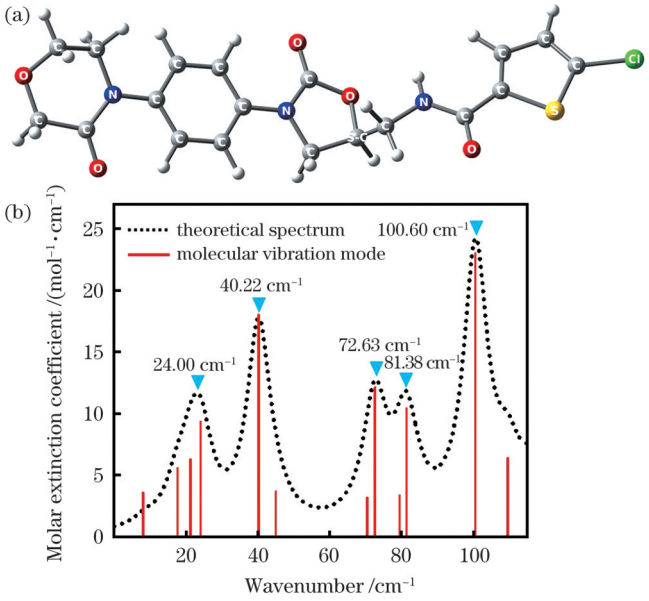

图1 拜瑞妥理论仿真结果。(a)分子模型;(b)理论光谱图

Fig. 1 Theoretical simulation results of Xarelto. (a) Molecular model; (b) theoretical spectral diagram

3.2 拜瑞妥的定性实验分析

通过理论分析预测拜瑞妥在0~100 cm^{-1}频段存在特征吸收谱线,接着本文通过远红外检测对拜瑞妥的远红外特征吸收特性进行实验分析,具体是对纯PE(参考)、拜瑞妥样品(分别含25 mg和60 mg拜瑞妥)进行定性实验分析。远红外检测原理如图2(a)中插图所示。采集到的信号时域图如图2(a)所示,其中点线为纯PE样品,实线为25 mg拜瑞妥样品,点直线为60 mg拜瑞妥样品。可以看出:1)各样品信号之间存在时移,压片越厚时移越明显,原因在于压片厚度越大,远红外辐射穿透压片所需的时间就越长;2)各样品的信号强度随着拜瑞妥质量的增加而衰减,原因在于拜瑞妥对远红外辐射的吸收强于PE对远红外辐射的吸收,压片中拜瑞妥含量越高,其对远红外辐射的吸收量就越多,表现为幅度衰减越大。

接着,对时域图进行傅里叶变换,得到频域图,如

图 2(b)所示。可以看出，在 10～120 cm^{-1}范围内，相对于纯 PE 的参考信号，拜瑞妥的样品信号存在三个明显吸收谱带，具体分别位于 40～55 cm^{-1}、70～85 cm^{-1}和 90～105 cm^{-1}处。

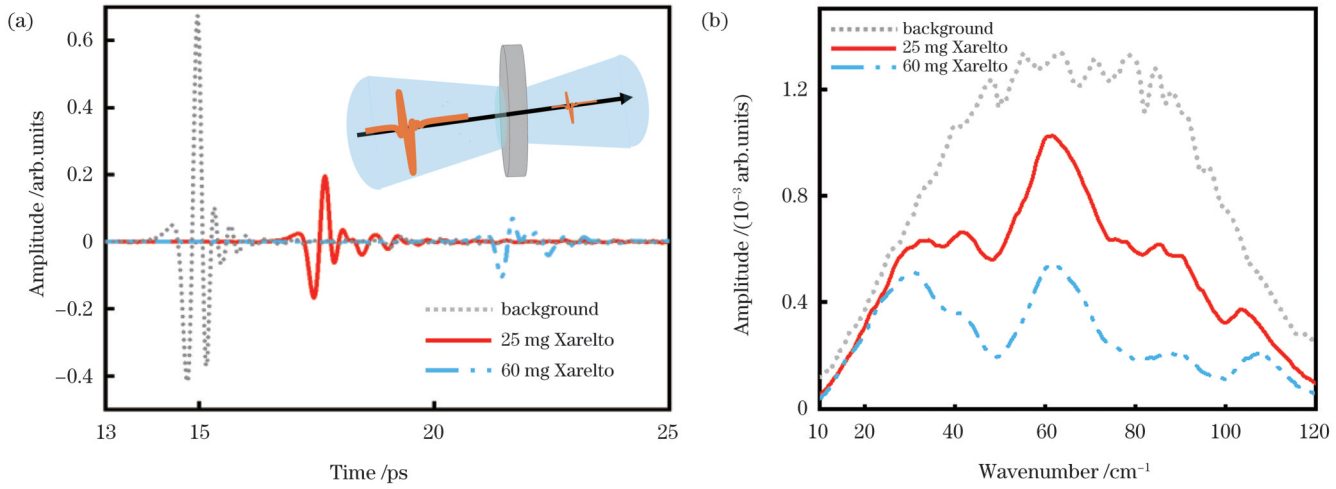

图 2　拜瑞妥定性检测的实验结果。(a)时域图，插图为检测示意图；(b)频域图

Fig. 2　Experimental results of qualitative detection of Xarelto. (a) Time domain diagram with schematic of detection shown in inset; (b) frequency domain diagram

为了更清晰地观察拜瑞妥的远红外特征吸收谱线，首先计算样品的吸光度，然后作吸收图谱。计算公式为

$$\alpha(w)=\lg\left[\frac{I_{ref}(w)}{I_{sam}(w)}\right], \tag{1}$$

式中：α为吸光度；w为波数；$I_{ref}(w)$为纯 PE 的频谱强度；$I_{sam}(w)$为拜瑞妥样品的频谱强度。当频率小于 20 cm^{-1}或大于 100 cm^{-1}时样品与 PE 频谱强度相近，导致计算得到的吸光度不准确，故仅对 20～100 cm^{-1}有效频域范围内的吸光度进行分析。如图 3 所示，拜瑞妥吸收谱在 49.03、80.54、96.29 cm^{-1}处出现吸收峰，在 38.87 cm^{-1}和 72.66 cm^{-1}处出现两个较弱的吸收肩峰。

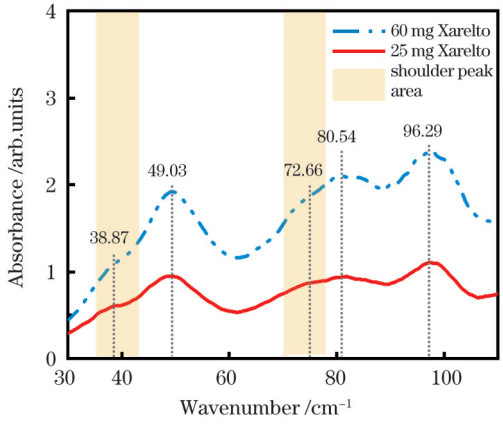

图 3　拜瑞妥的远红外特征吸收谱

Fig. 3　Far-infrared characteristic absorbance spectra of Xarelto

将实验吸收谱与理论仿真得到的特征吸收谱线进行比对，分析拜瑞妥远红外吸收特性对应的分子振动模式，详细对比结果如表 1 所示，其中 Ph 为苯环。由表 1 可知，拜瑞妥的理论仿真吸收谱线与实验谱图具有较高的一致性，各特征吸收峰的相对峰强一致，峰位偏差较小。38.87 cm^{-1}处肩峰的理论频率和实测频率偏差较大，主要原因在于仪器在低频处的噪声较大，对测试结果有一定干扰。

表 1　拜瑞妥理论峰与实测峰的对应关系以及相应的分子运动模式

Table 1　Corresponding relationship between theoretical peak and measured peak of Xarelto as well as corresponding molecular motion pattern

Theoretical peak	Measured peak	Deviation	Molecular motion pattern
24.00 cm^{-1} (shoulder peak)	38.87 cm^{-1} (shoulder peak)	14.870 cm^{-1}	Twisting (—$NC_4H_6O_2$)+ rocking (—CH_2—)+ rocking (—C_4H_2ClS)
40.22 cm^{-1}	49.03 cm^{-1}	8.810 cm^{-1}	Twisting (—$NC_4H_6O_2$)
72.63 cm^{-1} (shoulder peak)	72.66 cm^{-1} (shoulder peak)	0.030 cm^{-1}	Twisting (—$NC_4H_6O_2$)
81.38 cm^{-1}	80.54 cm^{-1}	0.084 cm^{-1}	Twisting (—Ph)+ twisting (—$NC_4H_6O_2$)
100.60 cm^{-1}	96.29 cm^{-1}	4.310 cm^{-1}	Rocking (—COC—)

利用 GaussView 软件对理论仿真结果进行图形化处理，观测拜瑞妥分子模型在 0～100 cm^{-1}频段内每一个特征吸收谱线下的基团运动模式，从而解析实测远红外特征吸收峰对应的分子运动模式。具体如下：

38.87 cm^{-1}肩峰对应 24.00 cm^{-1}理论峰，主要源于亚甲基的面内摇摆振动、噻吩衍生结构的面外摇摆振动和 N，O-六元杂环的面外卷曲振动的集合运动。49.03 cm^{-1}吸收峰对应 40.22 cm^{-1}理论峰，主要源于 N，O-五元杂环的面外卷曲振动，如图 4(a)虚线框所示。72.66 cm^{-1}肩峰对应 72.63 cm^{-1}理论峰，主要来源于酰胺键的面外卷曲振动。80.54 cm^{-1}吸收峰对应 81.38 cm^{-1}理论峰，主要源于苯环和 N，O-六元杂环的面外卷曲振动，如图 4(b)虚线框所示。96.29 cm^{-1}吸收峰对应 100.60 cm^{-1}理论峰，主要来源于 N，O-六元杂环中—CH_2—O—CH_2—的面内摇摆振动，如图 4(c)虚线框所示。

基于以上理论仿真和实验测试的结果，明确 38.87、49.03、72.66、80.54、96.29 cm^{-1}为拜瑞妥在 0～100 cm^{-1}内的特征峰，可用于该药物的定性识别。

3.3 拜瑞妥的定量实验分析

基于拜瑞妥的远红外吸收特性，本文进一步对其进行定量分析。对不同质量拜瑞妥的压片样品进行远红外光谱检测，选择 49.03、80.54、96.29 cm^{-1}作为定量指标，研究峰高随拜瑞妥质量的变化规律，结果如图 5(a)所示。进一步通过去基线操作，扣除基线对吸收光谱的影响，结果如图 5(b)所示。可以明显看出，随着拜瑞妥质量从 2.5 mg 逐渐递增至 25.0 mg，其远红外吸收峰强度逐渐上升。

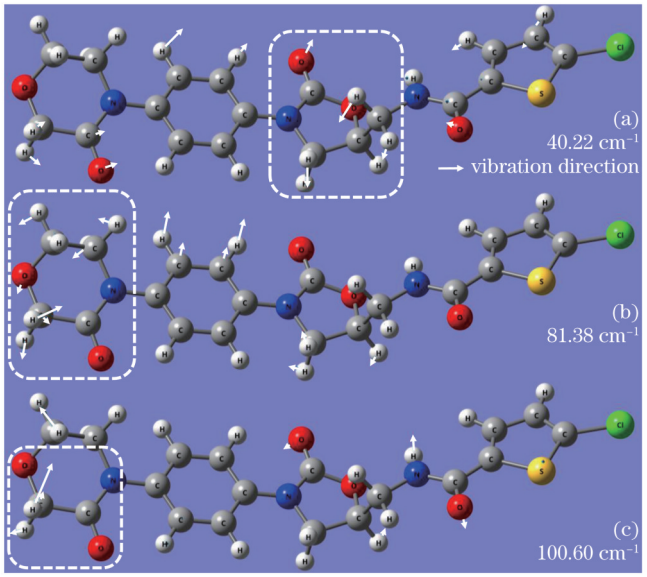

图 4 拜瑞妥在不同理论峰处的理论振动模式图。(a) 40.22 cm^{-1}；(b) 81.38 cm^{-1}；(c) 100.60 cm^{-1}

Fig. 4 Theoretical vibration modes of Xarelto at different theoretical peaks. (a) 40.22 cm^{-1}; (b) 81.38cm^{-1}; (c) 100.60 cm^{-1}

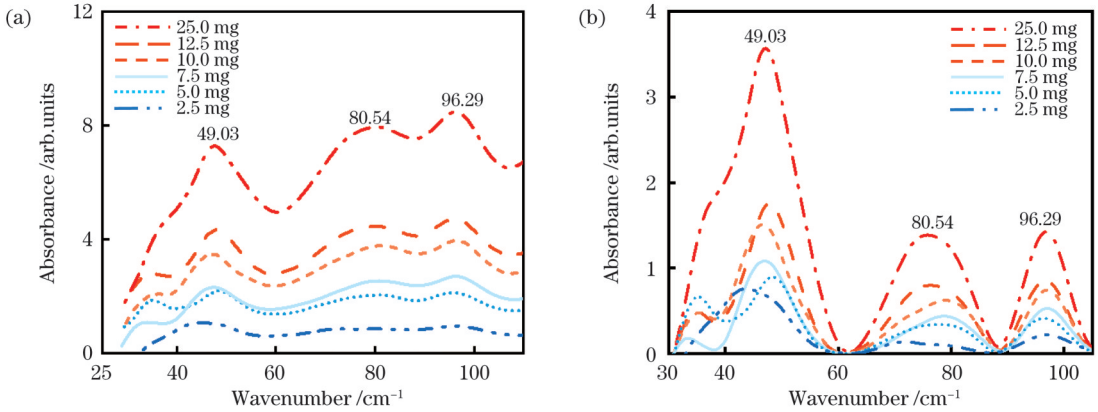

图 5 不同质量拜瑞妥样品的吸收图。(a)未去基线的吸收图；(b)去基线后的吸收图

Fig. 5 Absorption spectra of samples with different Xarelto masses. (a) Before baseline removal; (b) after baseline removal

接着通过测量三个强峰 49.03、80.54、96.29 cm^{-1}的峰高，对拜瑞妥进行定量分析。如图 6 所示，拜瑞妥的质量与其三个特征吸收峰峰高之间存在线性关系，符合 Beer-Lambert 定律。具体的线性拟合函数表达式为

$$\begin{cases} y_{49.03\ cm^{-1}} = 0.16067 + 0.13444x \\ R^2 = 0.99258 \\ S = 0.07253 \end{cases}, \tag{2}$$

$$\begin{cases} y_{96.29\ cm^{-1}} = 0.09964 + 0.05559x \\ R^2 = 0.99319 \\ S = 0.02587 \end{cases}, \tag{3}$$

$$\begin{cases} y_{80.54\ cm^{-1}} = 0.03228 + 0.0559x \\ R^2 = 0.99656 \\ S = 0.00888 \end{cases}, \tag{4}$$

式中：x为拜瑞妥的样本量；y为拜瑞妥远红外特征峰的吸光度，其下标为相应的远红外特征峰频率；R^2为相关系数；S为标准差。由上述结果可知：1) 80.54 cm^{-1}与 96.29 cm^{-1}处特征峰所对应的拟合直线的斜率相近，均小于 49.03 cm^{-1}处特征峰所对应的拟合直线的斜率，说明在拜瑞妥定量分析中，前两者特征峰的检测灵敏度相差不大，49.03 cm^{-1}处特征峰是检测灵敏度最高；2) 三个特征峰线性拟合的 R^2均大于 0.993，S均小于 0.026，说明线性拟合估计值与实测数据之间的拟合程度较高，即拟合结果的可靠性较高，定量估值误差率较低。因此，在拜瑞妥定量检测中，可通过多特征峰的联合定量分析来提高结果的准确率。

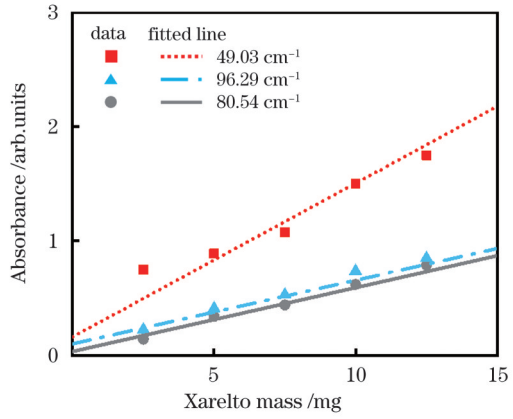

图 6 拜瑞妥质量与吸光度之间的关系

Fig. 6 Relationship between Xarelto mass and absorbance

4 结 论

基于密度泛函理论,使用远红外探测技术,对新型抗血栓药物拜瑞妥进行了光谱分析。通过理论仿真,预测拜瑞妥谱图在 100 cm^{-1}以下波数范围内存在 5 个特征峰,使用远红外检测技术采集到与理论预测高度一致的实验谱图,确定该药物的特征频率为 38.87、49.03、72.66、80.54、96.29 cm^{-1},并结合理论仿真结果分析了特征吸收峰对应的分子振动模式。在此基础上,对不同质量拜瑞妥药物进行了进一步检测分析,结果显示,特征吸收峰峰高随着拜瑞妥质量的增加呈线性递增的趋势(R^2均大于 0.993,S均小于 0.026)。基于多个特征峰与拜瑞妥质量的相关性可实现拜瑞妥的快速、定量检测。研究结果有助于推动拜瑞妥药物快速检测技术的发展。

参 考 文 献

[1] Clarke M, Green J S, Harper W M, et al. Screening for deep-venout hrombosis after hip and knee replacement without prophylaxis[J]. Journal of Bone and Joint Surgery, 1997, 79(5): 787-791.

[2] Freedman K B, Brookenthal K R, Fitzgerald R H, Jr, et al. A meta-analysis of thromboembolic prophylaxis following elective total hip arthroplasty[J]. The Journal of Bone and Joint Surgery, 2000, 82-A(7): 929-938.

[3] 曲洪雪, 刘云鹏. 骨科深静脉血栓形成危险因素及发病机制的研究进展[J]. 中国矫形外科杂志, 2009, 17(2): 110-112.
Qu H X, Liu Y P. Research progress on risk factors and pathogenesis of deep venous thrombosis in orthopedics[J]. Orthopedic Journal of China, 2009, 17(2): 110-112.

[4] 王敏, 孟硕, 郭江辉, 等. 肺动脉栓塞检测的可视中国人蒙特卡罗模拟分析[J]. 中国激光, 2022, 49(24): 2407103.
Wang M, Meng S, Guo J H, et al. Monte Carlo simulation analysis of pulmonary embolism detection by visual China people [J]. Chinese Journal of Lasers, 2022, 49(24): 2407103.

[5] Silverstein M D, Heit J A, Mohr D N, et al. Trends in the incidence of deep vein thrombosis and pulmonary embolism: a 25-year population-based study[J]. Archives of Internal Medicine, 1998, 158(6): 585-593.

[6] Perzborn E, Strassburger J, Wilmen A, et al. *In vitro* and *in vivo* studies of the novel antithrombotic agent BAY 59-7939: an oral, direct Factor Xa inhibitor[J]. Journal of Thrombosis and Haemostasis, 2005, 3(3): 514-521.

[7] Varin R, Mirshahi S, Mirshahi P, et al. Effect of rivaroxaban, an oral direct factor Xa inhibitor, on whole blood clot permeation and thrombolysis: critical role of red blood cells[J]. Blood, 2009, 114 (22): 1064.

[8] Mueck W, Lensing A W A, Agnelli G, et al. Rivaroxaban: population pharmacokinetic analyses in patients treated for acute deep-vein thrombosis and exposure simulations in patients with atrial fibrillation treated for stroke prevention[J]. Clinical Pharmacokinetics, 2011, 50(10): 675-686.

[9] Kubitza D, Becka M, Wensing G, et al. Safety, pharmacodynamics, and pharmacokinetics of BAY 59-7939—an oral, direct Factor Xa inhibitor—after multiple dosing in healthy male subjects[J]. European Journal of Clinical Pharmacology, 2005, 61(12): 873-880.

[10] 马云辉, 张寿. 骨科深静脉血栓形成药物预防的研究进展[J]. 中国现代医药杂志, 2010, 12(7): 134-136.
Ma Y H, Zhang S. Research progress on drug prevention of deep venous thrombosis in orthopedics[J]. Modern Medicine Journal of China, 2010, 12(7): 134-136.

[11] Kubitza D, Becka M, Voith B, et al. Safety, pharmacodynamics, and pharmacokinetics of single doses of BAY 59-7939, an oral, direct factor Xa inhibitor[J]. Clinical Pharmacology & Therapeutics, 2005, 78(4): 412-421.

[12] 朱忠勇. 凝血酶原时间和活化部分凝血活酶时间测定标准化(附纤维蛋白原测定推荐方法和淘汰过时的出凝血时间的建议)[J]. 中华医学检验杂志, 1998, 21(5): 308-312.
Zhu Z Y. Standardization of determination of prothrombin time and activated partial thromboplastin time (with recommended method of fibrinogen determination and suggestion of eliminating outdated clotting time)[J]. Chinese Journal of Laboratory Medicine, 1998, 21(5): 308-312.

[13] Lu Y Z, Feng L, Jiang X G, et al. Construction of a molecular structure model of mild-oxidized Chinese lignite using Gaussian09 based on data from FTIR, solid state ^{13}C-NMR[J]. Journal of Molecular Modeling, 2018, 24(6): 135.

[14] Jin Z M, Peng Y, Fang Y Q, et al. Photoinduced large polaron transport and dynamics in organic - inorganic hybrid lead halide perovskite with terahertz probes[J]. Light: Science & Applications, 2022, 11(1): 1-12.

[15] 施辰君, 吴旭, 彭滟. 太赫兹成像技术在肿瘤检测中的应用[J]. 光电工程, 2020, 47(5): 190638.
Shi C J, Wu X, Peng Y. Applications of terahertz imaging technology in tumor detection[J]. Opto-Electronic Engineering, 2020, 47(5): 190638.

[16] Peng Y, Huang J L, Luo J, et al. Three-step one-way model in terahertz biomedical detection[J]. PhotoniX, 2021, 2(1): 1-18.

[17] 朱亦鸣, 施辰君, 吴旭, 等. 生物医学检测中太赫兹光谱技术的算法研究[J]. 光学学报, 2021, 41(1): 0130001.
Zhu Y M, Shi C J, Wu X, et al. Terahertz spectroscopy algorithms for biomedical detection[J]. Acta Optica Sinica, 2021, 41(1): 0130001.

[18] 刘晓松, 赵国忠, 屈媛. 利用太赫兹光谱对四种肠胃药品的实验分析[J]. 激光与光电子学进展, 2023, 60(23): 2330001.
Liu X S, Zhao G S, Qu Y. Experimental analysis of four gastrointestinal drugs by terahertz spectroscopy[J]. Laser & Optoelectronics Progress, 2023, 60(23): 2330001.

[19] Rustichelli C, Gamberini G, Ferioli V, et al. Solid-state study of polymorphic drugs: carbamazepine[J]. Journal of Pharmaceutical and Biomedical Analysis, 2000, 23(1): 41-54.

[20] Zeitler J A. Pharmaceutical terahertz spectroscopy and imaging [M]//Müllertz A, Perrie Y, Rades T. Analytical techniques in the pharmaceutical sciences. Advances in delivery science and technology. New York: Springer, 2016: 171-222.

[21] Suresh K, Ashe J S, Matzger A J. Far-infrared spectroscopy as a probe for polymorph discrimination[J]. Journal of Pharmaceutical Sciences, 2019, 108(5): 1915-1920.

[22] Hakey P M, Allis D G, Ouellette W, et al. Cryogenic terahertz

spectrum of (+)-methamphetamine hydrochloride and assignment using solid-state density functional theory[J]. The Journal of Physical Chemistry A, 2009, 113(17): 5119-5127.

[23] Ruggiero M T, Bardon T, Strlič M, et al. Assignment of the terahertz spectra of crystalline copper sulfate and its hydrates via solid-state density functional theory[J]. The Journal of Physical Chemistry A, 2014, 118(43): 10101-10108.

[24] Kazachenko A S, Tomilin F N, Pozdnyakova A A, et al. Theoretical DFT interpretation of infrared spectra of biologically active arabinogalactan sulphated derivatives[J]. Chemical Papers, 2020, 74(11): 4103-4113.

[25] Wallace S, Lambrakos S G, Shabaev A, et al. IR absorption spectra for pesticides using density functional theory[J]. Proceedings of SPIE, 2022, 12091: 120910D.

Far Infrared Spectrum of Antithrombotic Drug Xarelto

Wei Xiaoke, Wu Xu*, Lu Xiaosen, Wang Junjie, Li Jingnan, Yang Yansi, Chu Xinbo, Wang Qiliang, Jin Zuanming, Peng Yan

College of Optical-Electrical and Computer Engineering, University of Shanghai for Science and Technology, Shanghai 200093, *China*

Abstract

Objective Deep venous thrombosis (DVT) is an orthopedic complication with an incidence rate ranging from 66% to 84%. When a thrombus dislodges, it can circulate through the bloodstream and obstruct blood vessels. In severe cases, this can lead to disability or even death in patients. Consequently, preventing thrombosis is a critical aspect of orthopedic treatment and is essential for patient recovery after surgery. Xarelto is currently the most widely used new oral anticoagulant in clinical practice. It achieves anticoagulation by inhibiting factor Xa in a combined state, reducing the risk of thrombosis by 30%. However, due to varying physiological conditions among patients, quantitative testing is necessary for individualized medication in clinical treatment to realize optimal therapeutic effects. Current quantitative measurement methods can be classified into direct and indirect measurement techniques. However, these methods have certain limitations, including high cost, accuracy issues, and controversy to a certain extent. They are also influenced by patients' physiological characteristics, instruments, and reagents. Consequently, researchers are seeking a novel testing method to enable rapid and quantitative analysis of Xarelto contents. Far-infrared radiation, with a wavelength of 25 μm to 1000 μm, is highly sensitive to related low-frequency vibrations or rotational information, such as changes in configuration, crystal structure, and molecular agglomeration. The far-infrared spectrum detection boasts low photon energy, high resolution, and broad spectral bandwidth, making it widely used in molecular qualitative identification and quantitative analysis. In this study, we examined the far-infrared spectral characteristics of Xarelto using theoretical simulation and experimental testing methods and performed quantitative analysis based on these characteristics. We analyzed the absorption frequency of Xarelto in the wavenumber range of 0-100 cm^{-1} and related molecular motion modes to predict its far-infrared absorption characteristics using density theory. By collecting Xarelto experimental absorption spectrum and employing Fourier far-infrared precision spectrometer, we compared the results with theoretical analyses. This revealed Xarelto characteristic peaks in the far-infrared band. By examining multiple characteristic peaks, we studied the absorption spectrum changes of Xarelto samples with different contents in the far-infrared band. We then analyzed the correlation between Xarelto content and peak intensity, ultimately achieving quantitative testing of Xarelto.

Methods This study utilized the PubChem Structure database to construct a molecular simulation model for Xarelto. We employed quantum chemical software Gaussian 09 and density functional theory to calculate and simulate Xarelto theoretical far-infrared spectral characteristics. Specifically, we selected the DFT/B3LYP/3-21G basis set to optimize and calculate the Xarelto molecular model, predicting its properties in the 0-100 cm^{-1} range and applying the Gaussian broadening of Xarelto spectral lines (with a full width at half-maximum of 4 cm^{-1}). We then used a far-infrared spectrometer to conduct qualitative experimental tests on pure polyethylene (PE) and 25 mg and 60 mg Xarelto samples. We also collected the far-infrared absorption maps of Xarelto/PE hybrid chips with Xarelto masses ranging from 2.5 mg to 25 mg for quantitative experiments.

Results and Discussions In this study, we obtained Xarelto theoretical spectrum through the theoretical simulation method (Fig. 1), which identified the peaks of Xarelto theoretical characteristics at 24.00, 40.22, 72.63, 81.38, and 100.60 cm^{-1}. Through qualitative experimental tests of pure PE and 25 mg and 60 mg Xarelto samples, we obtained the drug experimental far-infrared absorption diagram (Fig. 3), revealing absorption peaks at 49.03, 80.54, and 96.29 cm^{-1}, as well as two weak absorption shoulder peaks at 38.87 cm^{-1} and 72.66 cm^{-1}. The relative peaks are consistent, and peak deviation is minimal. Based on Xarelto far-infrared absorption characteristics, we selected 49.03, 80.54, and 96.29 cm^{-1} as quantitative indicators to examine the far infrared spectrum rules of different samples with different Xarelto masses (Fig. 5) and conducted a quantitative analysis. There is a linear relationship between Xarelto mass and the three feature absorption peak heights, which aligns with Beer-Lambert's law (Fig. 6). The specific expressions of the linear fitting functions are $y_{49.03\ cm^{-1}}=0.16067+0.13444x$ with a correlation coefficient of 0.99258 and a standard deviation of 0.07253, $y_{96.29\ cm^{-1}}=0.09964+0.05559x$ with a correlation coefficient of 0.99319 and standard deviation of 0.02587, and

$y_{80.54\ cm^{-1}}=0.03228+0.0559x$ with a correlation coefficient of 0.99656 and standard deviation of 0.008888. These results indicate that the linear fitting estimation values and measured data are highly consistent, and the reliability of the linear fitting trend line is substantial. In conducting proper quantitative tests for Xarelto, we can further improve the quantitative accuracy via multi-peak and quantitative analysis.

Conclusions Based on density functional theory, in this study, far-infrared detection technology was employed to analyze the novel oral anticoagulant Xarelto, examining its far-infrared spectral characteristics and conducting quantitative analysis using its characteristic absorption peaks. Through theoretical simulation, it was predicted that Xarelto exhibits five characteristic peaks within the wavenumber range below 100 cm^{-1}. Subsequently, we used far-infrared detection technology to collect experimental spectra consistent with the theoretical prediction results, determining the drug characteristic frequencies at 38.87, 49.03, 72.66, 80.54, and 96.29 cm^{-1}. Theoretical simulation results were combined to analyze the corresponding molecular vibration modes for these characteristic absorption peaks. Building on this foundation, different samples with different Xarelto masses were detected and analyzed. Furthermore, it was discovered that the characteristic absorption peak height increases linearly with the Xarelto mass (correlation coefficients are greater than 0.993, and standard deviations are less than 0.026). The correlation between multiple characteristic peaks and Xarelto masses enables rapid and quantitative testing of Xarelto contens. The findings of this study will contribute to the development of rapid detection methods for antithrombotic drugs like Xarelto in the future.

Key words medical optics; far-infrared spectrum; Xarelto; quantitative determination; density functional theory